

# Unsupervised Video Domain Adaptation: A Disentanglement Perspective

Pengfei Wei<sup>1</sup>, Lingdong Kong<sup>1,2</sup>, Xinghua Qu<sup>1</sup>, Xiang Yin<sup>1</sup>, Zhiqiang Xu<sup>3</sup>, Jing Jiang<sup>4</sup>, Zejun Ma<sup>1</sup>

<sup>1</sup>ByteDance AI Lab <sup>2</sup>National University of Singapore <sup>3</sup>MBZUAI <sup>4</sup>University of Technology Sydney  
 {pengfei.wei, xinghua.qu, yinxiang.stephen, mazejun}@bytedance.com  
 lingdong@comp.nus.edu.sg, zhiqiang.xu@mbzuai.ac.ae, jing.jiang@uts.edu.au  
<https://ldkong.com/TranSVAE>

## Abstract

Unsupervised video domain adaptation is a practical yet challenging task. In this work, for the first time, we tackle it from a disentanglement view. Our key idea is to disentangle the domain-related information from the data during the adaptation process. Specifically, we consider the generation of cross-domain videos from two sets of latent factors, one encoding the static domain-related information and another encoding the temporal and semantic-related information. A *Transfer Sequential VAE (TranSVAE)* framework is then developed to model such generation. To better serve for adaptation, we further propose several objectives to constrain the latent factors in *TranSVAE*. Extensive experiments on the UCF-HMDB, Jester, and Epic-Kitchens datasets verify the effectiveness and superiority of *TranSVAE* compared with several state-of-the-art methods. Code is publicly available<sup>1</sup>.

## 1 Introduction

Over the past decades, unsupervised domain adaptation (UDA) has attracted extensive research attention (Wilson and Cook 2020). Numerous UDA methods have been proposed and successfully applied to various real-world applications, *e.g.*, object recognition (Tzeng et al. 2017; Xiao and Zhang 2021; Zhang et al. 2022), semantic segmentation (Zou et al. 2018; Kong et al. 2021; Saporta et al. 2022), and object detection (Cai et al. 2019a; Guan et al. 2021; Yu et al. 2022). However, most of these methods and their applications are limited to the image domain, while much less attention has been devoted to video-based UDA, where the latter is undoubtedly more challenging.

Compared with image-based UDA, the source and target domains also differ temporally in video-based UDA. Images are spatially well-structured data, while videos are sequences of image frames with both spatial and temporal relations. Existing image-based UDA methods can hardly achieve satisfactory performance on the video-based UDA tasks as they fail to consider the temporal dependency of the video frames in handling the domain gaps. For instance, in video-based cross-domain action recognition tasks, domain gaps are presented by not only the actions of different per-

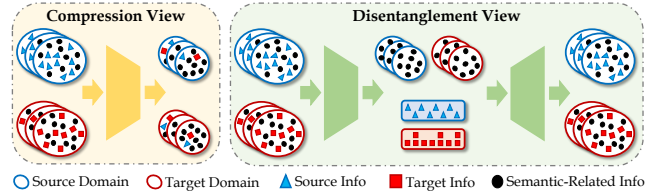



Figure 1: Conceptual comparisons between the traditional *compression view* and the proposed *disentanglement view*. Prior arts compress implicit domain information to obtain domain-indistinguishable representations; while in this work, we pursue explicit decouplings of domain-specific information from other information via generative modeling.

sons in different scenarios but also the actions that appear at different timestamps or last at different time lengths.

Recently, few works have been proposed for video-based UDA. The key idea of these methods is to achieve *temporal alignment* by aligning both frame- and video-level features through adversarial learning (Chen et al. 2019; Luo et al. 2020), contrastive learning (Turrissi et al. 2022; Sahoo et al. 2021), attention (Choi et al. 2020), or combining some of these mechanisms, *e.g.*, adversarial learning with attention (Pan et al. 2020; Chen, Gao, and Ma 2022). Though they have advanced video-based UDA, there is still room for improvement. Cross-domain videos are highly complex data, containing diverse information like domain-related information, semantic information, temporal information, *etc.* Existing works usually conduct feature alignments with diverse information mixed up, and thus may not guarantee that the source and target domains are sufficiently aligned.

Generally, prior methods follow a *compression* way to achieve adaptations (Fig. 1, ). With specifically-designed constraints, the domain-related information is highly compressed, making domains indistinguishable from the new representation, while the temporal and semantic-related information is adequately compressed so as to achieve good predictions using such new representation. However, as diverse information is mixed up, information confusion and loss are unavoidable during the compression, which may highly jeopardize the final adaptation performance. This motivates us to handle the video-based UDA from a *disentanglement* perspective. We aim at disentangling the domain in-

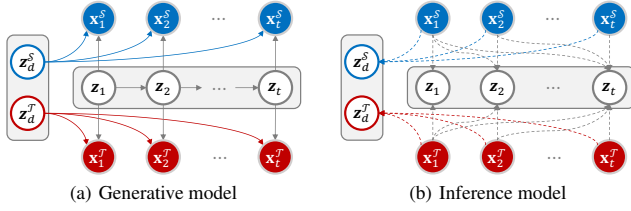


Figure 2: Graphical illustrations of the proposed *generative* and *inference* models for video domain disentanglement.

formation from the other information during the adaptation process (Fig. 1,  $\blacksquare$ ), such that the effect of domain discrepancy on the prediction task can be largely eliminated.

To achieve this goal, we first consider the *generation* process of cross-domain videos. We assume that a video sequence is generated from two sets of latent factors: one set consists of a sequence of random variables, which are *dynamic* over time and encode the semantic information that is related to the prediction task; the other set is *static* and introduces the domain-related information to the generated video. Fig. 2 illustrates the cross-domain video generation process. The blue/red nodes are the observed source/target videos  $\mathbf{x}^S/\mathbf{x}^T$ , respectively, over  $t$  timestamps. The static variables  $\mathbf{z}_d^S$  and  $\mathbf{z}_d^T$  follow a joint distribution and are *domain-specific*. Combining either of them with the dynamic variable  $\mathbf{z}_t$  at each timestamp, we can construct one frame data of a domain. Note that the sequences of the dynamic variables are shared across domains and are *domain-invariant*. They are also used for the final prediction task.

With the above generative model, we develop a **Transfer Sequential Variational AutoEncoder (TransVAE)** for video-based UDA. We design this novel VAE structure to model the cross-domain video generation process, and then leverage appropriate components to ensure that the disentanglement indeed serves the adaptation purpose. Firstly, we enable a good decoupling of the two sets of latent factors by minimizing their *mutual dependence*. This encourages the information in these two factor sets to be mutually exclusive. We then consider constraining each latent factor set. For sequences  $\mathbf{z}_t$  that are expected to be domain-invariant, we propose to align them across domains at both frame and video levels through *adversarial learning*. Meanwhile, we also add the *task-specific supervision* on  $\mathbf{z}_t$  extracted from source data (w/ ground-truth). Regarding  $\mathbf{z}_d^D$  with  $D \in \{S, T\}$  that are expected to be static and domain-specific, we propose a *contrastive triplet loss* on them. Note that  $\mathbf{z}_d^D$  should be naturally domain-specific as it is mutually independent with  $\mathbf{z}_t$ , which are constrained to be domain-invariant.

To the best of our knowledge, this is the first work that tackles the challenging video-based UDA from a domain disentanglement perspective. We conduct extensive experiments on popular benchmarks (UCF-HMDB, Jester, Epic-Kitchens, Sprites) and the results show that our *TransVAE* framework consistently outperforms previous state-of-the-art (SoTA) methods by large margins.

## 2 Related Work

**Unsupervised Video Domain Adaptation.** Despite the great progress in image-based UDA, only a few methods have recently attempted video-based UDA. In (Chen et al. 2019), a temporal attentive adversarial adaptation network (TA<sup>3</sup>N) is proposed to integrate a temporal relation module for temporal alignment. Choi et al. (2020) proposed a SAVA method using self-supervised clip order prediction and clip attention-based alignment. Based on a cross-domain co-attention mechanism, the temporal co-attention network TCoN (Pan et al. 2020) focuses on common key frames across domains for better alignment. Luo et al. (2020) pay more attention to the domain-agnostic classifier by using a network topology of the bipartite graph to model the cross-domain correlations. Instead of using adversarial learning, Sahoo et al. (2021) develop an end-to-end temporal contrastive learning framework named CoMix with background mixing and target pseudo-labels. Recently, Chen, Gao, and Ma (2022) learn multiple domain discriminators for multi-level temporal attentive features to achieve better alignment, while Turrissi et al. (2022) exploit two-headed deep architecture to learn a more robust target classifier by the combination of cross-entropy and contrastive losses. Although these methods have advanced video-based UDA, they align features with diverse information mixed up from a compression perspective, which leaves room for further improvement.

**Multi-Modal Video Adaptation.** Most recently, there are also a few works integrating multiple modality data for video-based UDA. Although we only use the single modality RGB features, we still discuss this multi-modal research line for a complete literature review. The very first work exploring the multi-modal nature of videos for UDA is MM-SADA (Munro and Damen 2020), where the correspondence of multiple modalities is exploited as a self-supervised alignment in addition to adversarial alignment. A later work, spatial-temporal contrastive domain adaptation (STCDA) (Song et al. 2021), utilizes a video-based contrastive alignment as the multi-modal domain metric to measure the video-level discrepancy across domains. Kim et al. (2021) propose cross-modal and cross-domain contrastive losses to handle feature spaces across modalities and domains. Yang et al. (2022) leverage both cross-modal complementarity and cross-modal consensus to learn the most transferable features through a CIA framework. It is worth noting that the proposed *TransVAE* – although only uses single modality RGB features – surprisingly achieves better UDA performance compared to the current state-of-the-art multi-modal method CIA, which highlights our superiority.

**Disentanglement.** Feature disentanglement is a wide and hot research topic. We only focus on works that are closely related to ours. In the image domain, some works consider adaptation from a generative view. Cai et al. (2019b) learn a disentangled semantic representation across domains. A similar idea is then applied to graph domain adaptation (Cai et al. 2021) and domain generalization (Ilse et al. 2020). (Deng et al. 2021) propose a novel informative feature disentanglement, equipped with the adversarial network or the metric discrepancy model. Another disentanglement-related topic is sequential data generation. To generate videos, exist-

ing works (Li and Mandt 2018; Zhu et al. 2020; Bai, Wang, and Gomes 2021) extend VAE to a recurrent form with different recursive structures. In this paper, we present a VAE-based structure to generate cross-domain videos. We aim at tackling the challenging video-based UDA from a new perspective: sequential domain disentanglement and transfer.

### 3 Technical Approach

Formally, for a typical video-based UDA problem, we have two domains, namely source domain  $\mathcal{S}$  and target domain  $\mathcal{T}$ . Domain  $\mathcal{S}$  contains sufficient labeled video sequences, denoted as  $\{(\mathbf{V}_i^{\mathcal{S}}, y_i^{\mathcal{S}})\}_{i=1}^{N_{\mathcal{S}}}$ , where  $\mathbf{V}_i^{\mathcal{S}}$  is a video sequence and  $y_i^{\mathcal{S}}$  is the class label. Domain  $\mathcal{T}$  consists of unlabeled video sequences, denoted as  $\{\mathbf{V}_i^{\mathcal{T}}\}_{i=1}^{N_{\mathcal{T}}}$ . For a sequence  $\mathbf{V}_i^{\mathcal{D}}$  from domain  $\mathcal{D} \in \{\mathcal{S}, \mathcal{T}\}$ , it contains  $T$  frames  $\{\mathbf{x}_{i,1}^{\mathcal{D}}, \dots, \mathbf{x}_{i,T}^{\mathcal{D}}\}$  in total<sup>2</sup>. We further denote  $N = N^{\mathcal{S}} + N^{\mathcal{T}}$ . The domains  $\mathcal{S}$  and  $\mathcal{T}$  are of different distributions but are sharing the same label space. The objective is to utilize both  $\{(\mathbf{V}_i^{\mathcal{S}}, y_i^{\mathcal{S}})\}_{i=1}^{N_{\mathcal{S}}}$  and  $\{\mathbf{V}_i^{\mathcal{T}}\}_{i=1}^{N_{\mathcal{T}}}$  to train a good classifier for domain  $\mathcal{T}$ .

**Framework Overview.** We adopt a VAE-based structure to model the cross-domain video generation process as shown in Fig. 2, and propose four constraints to regulate the two sets of latent factors. The reconstruction process is based on these two latent factors, *i.e.*,  $\mathbf{z}_1^{\mathcal{D}}, \dots, \mathbf{z}_T^{\mathcal{D}}$  and  $\mathbf{z}_d^{\mathcal{D}}$  that are sampled from the posteriors  $q(\mathbf{z}_t^{\mathcal{D}}|\mathbf{x}_{< t}^{\mathcal{D}})$  and  $q(\mathbf{z}_d^{\mathcal{D}}|\mathbf{x}_{1:T}^{\mathcal{D}})$ , respectively. The overall architecture consists of five segments including the encoder, LSTM, latent spaces, sampling, and decoder, as shown in Fig. 3. To better disentangle the domain information and facilitate the adaptation task, we propose four objective losses, namely *mutual information loss*, *domain adversarial loss*, *task supervision loss*, and *contrastive triplet loss*. The mutual information loss works on  $q(\mathbf{z}_t^{\mathcal{D}}|\mathbf{x}_{< t}^{\mathcal{D}})$  and  $q(\mathbf{z}_d^{\mathcal{D}}|\mathbf{x}_{1:T}^{\mathcal{D}})$  to maximize the independence of the two latent factor sets. The domain adversarial loss constrains the dynamic latent factors to be domain-invariant, *i.e.*, one cannot distinguish domains using  $\mathbf{z}_1^{\mathcal{D}}, \dots, \mathbf{z}_T^{\mathcal{D}}$ . With the two losses, the static latent factors  $\mathbf{z}_d^{\mathcal{D}}$  naturally encode the domain-related information. To further enhance the domain specificity, we put a contrastive triplet loss on  $\mathbf{z}_d^{\mathcal{D}}$ . By doing so, we also guarantee that  $\mathbf{z}_d^{\mathcal{D}}$  are time-invariant. At last, as domain  $\mathcal{S}$  has labels, we build a prediction network using  $\mathbf{z}_1^{\mathcal{S}}, \dots, \mathbf{z}_T^{\mathcal{S}}$ . In the adaptation phase, we extract the dynamic representations of the target test video sequences, and then pass them to the prediction network. Next, we elaborate the technical details of each component in *TransVAE*.

**Video Sequence Reconstruction.** The overall architecture of *TransVAE* follows a VAE-based structure (Li and Mandt 2018; Zhu et al. 2020; Bai, Wang, and Gomes 2021) with two sets of latent factors  $\mathbf{z}_1^{\mathcal{D}}, \dots, \mathbf{z}_T^{\mathcal{D}}$  and  $\mathbf{z}_d^{\mathcal{D}}$ . The generative and inference graphical models are presented in Fig. 2(a) and 2(b), respectively. Similar to the conventional VAE, we use a standard Gaussian distribution for static latent factors. For dynamic ones, we use a sequential prior  $\mathbf{z}_t^{\mathcal{D}}|\mathbf{z}_{< t}^{\mathcal{D}} \sim \mathcal{N}(\boldsymbol{\mu}_t, \text{diag}(\boldsymbol{\sigma}_t^2))$ , that is, the prior distribution of the current

dynamic factor is conditioned on the historical dynamic factors. The distribution parameters can be re-parameterized as a recurrent network, *e.g.*, LSTM, with all previous dynamic latent factors as the input. Denoting  $\mathbf{Z}^{\mathcal{D}} = \{\mathbf{z}_1^{\mathcal{D}}, \dots, \mathbf{z}_T^{\mathcal{D}}\}$  for simplification, we then get the prior as follows:

$$p(\mathbf{z}_d^{\mathcal{D}}, \mathbf{Z}^{\mathcal{D}}) = p(\mathbf{z}_d^{\mathcal{D}}) \prod_{t=1}^T p(\mathbf{z}_t^{\mathcal{D}}|\mathbf{z}_{< t}^{\mathcal{D}}). \quad (1)$$

Following Fig. 2(a),  $\mathbf{x}_t^{\mathcal{D}}$  is generated from  $\mathbf{z}_d^{\mathcal{D}}$  and  $\mathbf{z}_t^{\mathcal{D}}$ , and we thus model  $p(\mathbf{x}_t^{\mathcal{D}}|\mathbf{z}_d^{\mathcal{D}}, \mathbf{z}_t^{\mathcal{D}}) = \mathcal{N}(\boldsymbol{\mu}'_t, \text{diag}(\boldsymbol{\sigma}'_t{}^2))$ . The distribution parameters are re-parameterized by the decoder which can be flexible networks like the deconvolutional neural network. Using  $\mathbf{V}^{\mathcal{D}} = \{\mathbf{x}_1^{\mathcal{D}}, \dots, \mathbf{x}_T^{\mathcal{D}}\}$ , the *generation* can be formulated as:

$$p(\mathbf{V}^{\mathcal{D}}) = p(\mathbf{z}_d^{\mathcal{D}}) \prod_{t=1}^T p(\mathbf{x}_t^{\mathcal{D}}|\mathbf{z}_d^{\mathcal{D}}, \mathbf{z}_t^{\mathcal{D}}) p(\mathbf{z}_t^{\mathcal{D}}|\mathbf{z}_{< t}^{\mathcal{D}}). \quad (2)$$

Following Fig. 2(b), we model the posterior distributions of the latent factors as another two Gaussian distributions, *i.e.*,  $q(\mathbf{z}_d^{\mathcal{D}}|\mathbf{V}^{\mathcal{D}}) = \mathcal{N}(\boldsymbol{\mu}_d, \text{diag}(\boldsymbol{\sigma}_d^2))$  and  $q(\mathbf{z}_t^{\mathcal{D}}|\mathbf{x}_{< t}^{\mathcal{D}}) = \mathcal{N}(\boldsymbol{\mu}''_t, \text{diag}(\boldsymbol{\sigma}''_t{}^2))$ . The parameters of these two distributions are re-parameterized by the encoder, which can be a convolutional or LSTM module. However, the network of the static latent factors uses the whole sequence as the input while that of the dynamic latent factors only uses previous frames. Then the *inference* can be factorized as:

$$q(\mathbf{z}_d^{\mathcal{D}}, \mathbf{Z}^{\mathcal{D}}|\mathbf{V}^{\mathcal{D}}) = q(\mathbf{z}_d^{\mathcal{D}}|\mathbf{V}^{\mathcal{D}}) \prod_{t=1}^T q(\mathbf{z}_t^{\mathcal{D}}|\mathbf{x}_{< t}^{\mathcal{D}}). \quad (3)$$

Combining the above generation and inference process, we obtain the sequential VAE related objective function as:

$$\begin{aligned} \mathcal{L}_{\text{vae}} = & \mathbb{E}_{q(\mathbf{z}_d^{\mathcal{D}}, \mathbf{Z}^{\mathcal{D}}|\mathbf{V}^{\mathcal{D}})} \left[ - \sum_{t=1}^T \log p(\mathbf{x}_t^{\mathcal{D}}|\mathbf{z}_d^{\mathcal{D}}, \mathbf{z}_t^{\mathcal{D}}) \right] + \\ & \sum_{t=1}^T \text{KL}(q(\mathbf{z}_d^{\mathcal{D}}|\mathbf{V}^{\mathcal{D}}) || p(\mathbf{z}_d^{\mathcal{D}})) + \sum_{t=1}^T \text{KL}(q(\mathbf{z}_t^{\mathcal{D}}|\mathbf{x}_{< t}^{\mathcal{D}}) || p(\mathbf{z}_t^{\mathcal{D}}|\mathbf{z}_{< t}^{\mathcal{D}})), \end{aligned} \quad (4)$$

which is a frame-wise negative variational lower bound.

**Mutual Dependence Minimization** (Fig. 3, ■). Only using the above disentanglement model cannot guarantee that the static latent factors are encoding the domain-related information and the dynamic latent factors are encoding the temporal and semantic-related information. Considering that the *static* latent factors are expected to be domain-specific while the *dynamic* latent factors are in the opposite, we first enforce the two sets of latent factors to be mutually independent. To do so, we introduce the mutual information loss  $\mathcal{L}_{\text{mi}}$  to regulate the two sets of latent factors. Mutual information (Batina et al. 2011) is formally defined as the KL divergence of the joint distribution to the product of the marginal distri-

<sup>2</sup>Without confusion, we omit the subscript  $i$  to represent a video sequence  $\mathbf{V}^{\mathcal{D}}$  and the corresponding notations, *e.g.*,  $\{\mathbf{x}_1^{\mathcal{D}}, \dots, \mathbf{x}_T^{\mathcal{D}}\}$ .

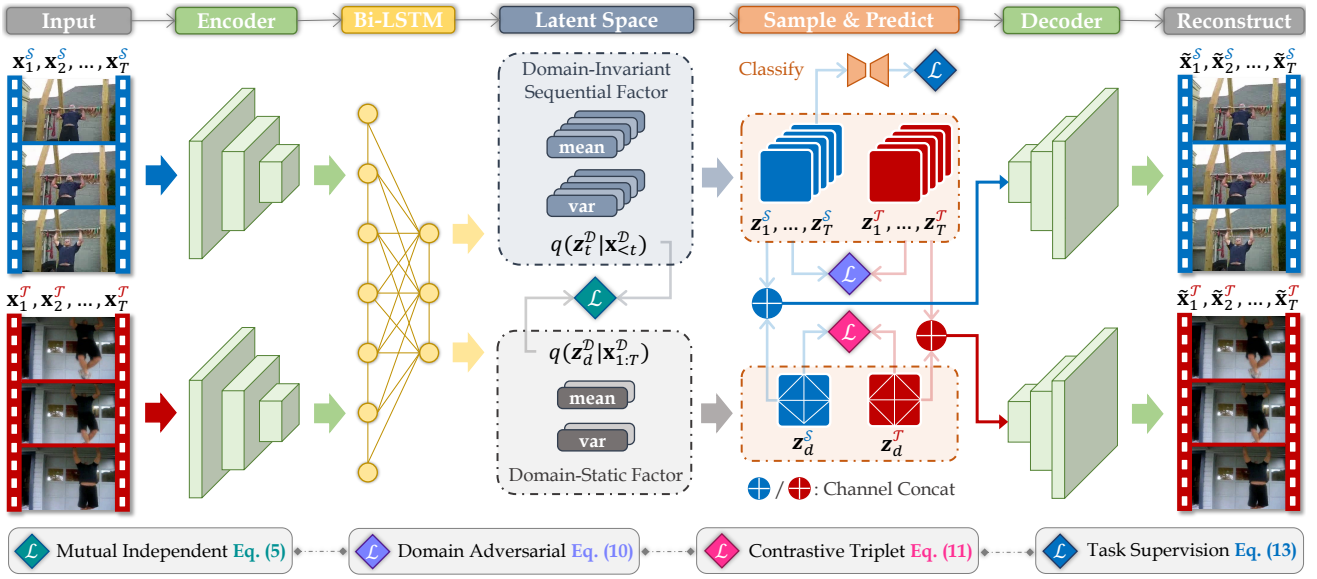


Figure 3: *TranSVAE* overview. The input videos are fed into an encoder to extract the visual features, followed by an LSTM to explore the temporal information. Two groups of *mean* and *variance* networks are then applied to model the posterior of the latent factors, i.e.,  $q(\mathbf{z}_t^D | \mathbf{x}_{<t}^D)$  and  $q(\mathbf{z}_d^D | \mathbf{x}_{1:T}^D)$ . The new representations  $\mathbf{z}_1^D, \dots, \mathbf{z}_T^D$  and  $\mathbf{z}_d^D$  are sampled, and then concatenated and passed to a decoder for reconstruction. Four constraints are proposed to regulate the latent factors for adaptation purposes.

bution of each variable. Thus, we obtain:

$$\begin{aligned} \mathcal{L}_{mi}(\mathbf{z}_d^D, \mathbf{Z}^D) &= \sum_{t=1}^T \text{KL}(q(\mathbf{z}_d^D, \mathbf{z}_t^D) || q(\mathbf{z}_d^D)q(\mathbf{z}_t^D)) \\ &= \sum_{t=1}^T [H(\mathbf{z}_d^D) + H(\mathbf{z}_t^D) - H(\mathbf{z}_d^D, \mathbf{z}_t^D)]. \end{aligned} \quad (5)$$

To calculate Eq. (5), we need to estimate the densities of  $\mathbf{z}_d^D, \mathbf{z}_t^D$  and  $(\mathbf{z}_d^D, \mathbf{z}_t^D)$ . Based on (Chen et al. 2018), we use the mini-batch weighted sampling as follows:

$$\begin{aligned} H(\mathbf{z}) &= -\mathbb{E}_{q(\mathbf{z})}[\log q(\mathbf{z})] \\ &\approx -\log \frac{1}{M} \sum_{i=1}^M \left[ \log \frac{1}{MN} \sum_{j=1}^M q(\mathbf{z}(\mathbf{x}_i) | \mathbf{x}_j) \right], \end{aligned} \quad (6)$$

where  $\mathbf{z}$  is  $\mathbf{z}_d^D, \mathbf{z}_t^D$  or  $(\mathbf{z}_d^D, \mathbf{z}_t^D)$ ,  $N$  denotes the data size and  $M$  is the mini-batch size. As discussed in (Chen et al. 2018), such an estimator is biased, but computing it does not require any additional hyperparameters.

**Domain Temporal Alignment** (Fig. 3, ■). We now consider enforcing the *dynamic* latent factors to be domain-invariant. Similar to the image-based UDA, we propose to reduce the domain gaps between the cross-domain dynamic latent factors. There are several ways to achieve this, and in this paper, we take advantage of the most popular adversarial-based idea (Ganin et al. 2016). Specifically, we build a domain classifier to discriminate whether the data is from the source domain or the target domain. When back-propagating the gradients, a gradient reversal layer (GRL) is adopted to invert the gradients. Like existing video-based

UDA methods, we also conduct both frame-level and video-level alignments. As TA<sup>3</sup>N (Chen et al. 2019) does, we exploit the temporal relation network (TRN) (Zhou et al. 2018) to discover the temporal relations among different frames, and then aggregate all the temporal relation features into the final video-level features. This enables another level of alignment on the temporal relation features. Thus, we have:

$$\mathcal{L}_f = \frac{1}{N} \sum_{i=1}^N \frac{1}{T} \sum_{t=1}^T CE[G_f(\mathbf{z}_{i,t}^D), d_i], \quad (7)$$

$$\mathcal{L}_r = \frac{1}{N} \sum_{i=1}^N \frac{1}{T-1} \sum_{n=2}^T CE[G_r(TrN_n(\mathbf{Z}_i^D)), d_i], \quad (8)$$

$$\mathcal{L}_v = \frac{1}{N} \sum_{i=1}^N CE \left[ G_v \left( \frac{1}{T-1} \sum_{n=2}^T TrN_n(\mathbf{Z}_i^D) \right), d_i \right], \quad (9)$$

where  $d_i$  is the domain label,  $CE$  denotes the cross-entropy loss function,  $\mathbf{Z}_i^D = \{\mathbf{z}_{i,1}^D, \dots, \mathbf{z}_{i,T}^D\}$ ,  $TrN_i$  is the  $n$ -frame temporal relation network,  $G_f$ ,  $G_r$ , and  $G_v$  are the frame level, the temporal relation feature level, and the video feature level domain classifiers, respectively. Note that the other ways of integrating frame-level features to video-level features, e.g., using a Graph Convolutional Network (GCN) (Wang and Gupta 2018) as (Sahoo et al. 2021) do, can be straightforwardly applied here. To this end, we obtain the domain adversarial loss by summing up Eqs. (7-9):

$$\mathcal{L}_{adv} = \mathcal{L}_f + \mathcal{L}_r + \mathcal{L}_v. \quad (10)$$

We assign equal importance for these three levels of losses to reduce the overhead of the hyperparameter search.



**Domain Specificity & Static Consistency** (Fig. 3, ■). With  $\mathcal{L}_{\text{mi}}$  and  $\mathcal{L}_{\text{adv}}$ , the dynamic latent factors are enforced to be domain-invariant, and independent of the static latent factors. Naturally, the static latent factors should encode the domain-specific information. However, we further notice that the characteristics of the domain specificity should be statically consistent over dynamic frames. Thus, we hope that  $\mathbf{z}_d^{\mathcal{D}}$  does not change a lot when  $\mathbf{z}_t^{\mathcal{D}}$  varies over time. To achieve this, given a sequence, we randomly shuffle the temporal order of frames to form a new sequence. The static latent factors disentangled from the original sequence and the shuffled sequence should be ideally equal or be very close at least. This motivates us to minimize the distance between these two static factors. Meanwhile, to further enhance the domain specificity, we enforce the dynamic latent factors from different domains to have a large distance. To this end, we propose the following contrastive triplet loss:

$$\mathcal{L}_{\text{ctc}} = \max \left( D(\mathbf{z}_d^{\mathcal{D}^+}, \tilde{\mathbf{z}}_d^{\mathcal{D}^+}) - D(\mathbf{z}_d^{\mathcal{D}^+}, \mathbf{z}_d^{\mathcal{D}^-}) + \mathbf{m}, 0 \right), \quad (11)$$

where  $D(\cdot, \cdot)$  denotes the Euclidean distance,  $\mathbf{m}$  is the margin set to 1 in the experiments,  $\mathbf{z}_d^{\mathcal{D}^+}$ ,  $\tilde{\mathbf{z}}_d^{\mathcal{D}^+}$ , and  $\mathbf{z}_d^{\mathcal{D}^-}$  are static latent factors of the anchor sequence from domain  $\mathcal{D}^+$ , the shuffled sequence, and a randomly selected sequence from domain  $\mathcal{D}^-$ , respectively. Note that  $\mathcal{D}^+$  and  $\mathcal{D}^-$  represent two different domains.

**Task-Specific Supervision** (Fig. 3, ■). We further encourage the dynamic latent factors to carry the semantic information. Considering that the source domain has sufficient labels, we accordingly design the task supervision as the regularization imposed on  $\mathbf{z}_t^{\mathcal{S}}$ . This gives us:

$$\mathcal{L}_{\text{cls}} = \frac{1}{N^{\mathcal{S}}} \sum_{i=1}^{N^{\mathcal{S}}} \mathcal{L}(\mathcal{F}(\mathbf{z}_i^{\mathcal{S}}), y_i^{\mathcal{S}}), \quad (12)$$

where  $\mathcal{F}(\cdot)$  is the feature transformer mapping the frame-level features to video-level features, specifically TRN used in this paper, and  $\mathcal{L}(\cdot, \cdot)$  can be either cross-entropy loss or mean squared error loss according to the task.

Although the dynamic latent factors are constrained to be domain-invariant, we do not completely rely on source semantics to learn features discriminative for the target domain. We propose to incorporate target pseudo-labels in task specific supervision. During the training, we use the prediction network obtained in the previous epoch to generate the target pseudo-labels of the unlabelled target training data for the current epoch. However, to increase the reliability of target pseudo-labels, we let the prediction network be trained only on the source supervision for several epochs, and then integrate the target pseudo-labels in the following training epochs. Meanwhile, a confidence threshold is set to determine whether to use the target pseudo-labels or not. Thus, we have the final task-specific supervision as follows:

$$\mathcal{L}_{\text{cls}} = \frac{1}{N} \left( \sum_{i=1}^{N^{\mathcal{S}}} \mathcal{L}(\mathcal{F}(\mathbf{z}_i^{\mathcal{S}}), y_i^{\mathcal{S}}) + \sum_{i=1}^{N^{\mathcal{T}}} \mathcal{L}(\mathcal{F}(\mathbf{z}_i^{\mathcal{T}}), \tilde{y}_i^{\mathcal{T}}) \right), \quad (13)$$

where  $\tilde{y}_i^{\mathcal{T}}$  is the pseudo-label of  $\mathbf{z}_i^{\mathcal{T}}$ .

**Summary.** To this end, we reach the final objective function of our *TransVAE* framework as follows:

$$\mathcal{L}' = \mathcal{L}_{\text{svae}} + \lambda_1 \mathcal{L}_{\text{mi}} + \lambda_2 \mathcal{L}_{\text{adv}} + \lambda_3 \mathcal{L}_{\text{ctc}} + \lambda_4 \mathcal{L}_{\text{cls}}, \quad (14)$$

where  $\lambda_i, i = 1, 2, 3, 4$  denotes the loss balancing weight.

## 4 Experiments

In this section, we conduct extensive experimental studies on popular video-based UDA benchmarks to verify the effectiveness of the proposed *TransVAE* framework.

### 4.1 Datasets

**UCF-HMDB** is constructed by collecting the relevant and overlapping action classes from UCF<sub>101</sub> (Soomro, Zamir, and Shah 2012) and HMDB<sub>51</sub> (Kuehne et al. 2011). It contains 3,209 videos in total with 1,438 training videos and 571 validation videos from UCF<sub>101</sub>, and 840 training videos and 360 validation videos from HMDB<sub>51</sub>. This in turn gives two video-based UDA tasks:  $\mathbf{U} \rightarrow \mathbf{H}$  and  $\mathbf{H} \rightarrow \mathbf{U}$ .

**Jester** (Materzynska et al. 2019) consists of 148,092 videos of humans performing hand gestures. Pan et al. (2020) construct a large-scale cross-domain benchmark with 7 gesture classes, and form a single transfer task  $\mathbf{J}_{\mathcal{S}} \rightarrow \mathbf{J}_{\mathcal{T}}$ , where  $\mathbf{J}_{\mathcal{S}}$  and  $\mathbf{J}_{\mathcal{T}}$  contain 51,498 and 51,415 video clips, respectively.

**Epic-Kitchens** (Damen et al. 2018) is a challenging ego-centric dataset consisting of videos capturing daily activities in kitchens. Munro and Damen (2020) construct three domains across the eight largest actions. They are  $\mathbf{D}_1$ ,  $\mathbf{D}_2$ , and  $\mathbf{D}_3$  corresponding to P08, P01, and P22 kitchens of the full dataset, resulting in six cross-domain tasks in-between them.

**Sprites** (Li and Mandt 2018) contains sequences of animated cartoon characters with 15 action categories. The appearances of characters are fully controlled by four attributes, *i.e.*, body, top, bottom, and hair. We construct two domains,  $\mathbf{P}_1$  and  $\mathbf{P}_2$ .  $\mathbf{P}_1$  uses the *human* body with attributes randomly selected from 3 tops, 4 bottoms, and 5 hairs, while  $\mathbf{P}_2$  uses the *alien* body with attributes randomly selected from 4 tops, 3 bottoms, and 5 hairs. The attribute pools are non-overlapping across domains, resulting in completely heterogeneous  $\mathbf{P}_1$  and  $\mathbf{P}_2$ . Each domain has 900 video sequences and each sequence contains 8 frames.

### 4.2 Implementation Details

**Architecture.** Following the latest works (Sahoo et al. 2021; Turrissi et al. 2022), we use I3D (Carreira and Zisserman 2017) as the backbone. However, different from CoMix which jointly trains the backbone, we simply use the pre-trained I3D model on Kinetics (Kay et al. 2017), provided by (Carreira and Zisserman 2017), to extract RGB features. For the first three benchmarks, RGB features are used as the input of *TransVAE*. For Sprites, we use the original image as the input, for the purpose of visualizing the reconstruction and disentanglement results. We use the shared encoder and decoder structures across the source and target domains. For RGB feature inputs, the encoder and decoder are fully-connected layers. For original image inputs, the encoder and decoder are the convolution and deconvolution layers (from DCGAN (Yu et al. 2017)), respectively. For the TRN model,

Table 1: UDA performance comparisons on UCF-HMDB.

Method & Year	Backbone	U $\rightarrow$ H	H $\rightarrow$ U	Average $\uparrow$
DANN (JMLR'16)	ResNet-101	75.28	76.36	75.82
JAN (ICML'17)	ResNet-101	74.72	76.69	75.71
AdaBN (PR'18)	ResNet-101	72.22	77.41	74.82
MCD (CVPR'18)	ResNet-101	73.89	79.34	76.62
TA <sup>3</sup> N (ICCV'19)	ResNet-101	78.33	81.79	80.06
ABG (MM'20)	ResNet-101	79.17	85.11	82.14
TCoN (AAAI'20)	ResNet-101	87.22	89.14	88.18
MA <sup>2</sup> L-TD (WACV'22)	ResNet-101	85.00	86.59	85.80
Source-only ( $\mathcal{S}_{\text{only}}$ )	I3D	80.27	88.79	84.53
DANN (JMLR'16)	I3D	80.83	88.09	84.46
ADDA (CVPR'17)	I3D	79.17	88.44	83.81
TA <sup>3</sup> N (ICCV'19)	I3D	81.38	90.54	85.96
SAVA (ECCV'20)	I3D	82.22	91.24	86.73
CoMix (NeurIPS'21)	I3D	86.66	93.87	90.22
CO <sup>2</sup> A (WACV'22)	I3D	87.78	95.79	91.79
<b>TransVAE (Ours)</b>	<b>I3D</b>	<b>87.78</b>	<b>98.95</b>	<b>93.37</b>
Supervised-target ( $\mathcal{T}_{\text{sup}}$ )	I3D	95.00	96.85	95.93

we directly use the one provided by (Chen et al. 2019). Other details on this aspect are placed in Appendix.

**Configurations.** Our *TransVAE* is implemented with PyTorch. We use Adam with a weight decay of  $1e^{-4}$  as the optimizer. The learning rate is initially set to be  $1e^{-3}$  and follows a commonly used decreasing strategy in (Ganin et al. 2016). The batch size and the learning epoch is uniformly set to be 128 and 1,000, respectively, for all the experiments. We uniformly set 100 epochs of training under only source supervisions and involve the target pseudo-labels afterward. Following the common protocol in video-based UDA (Turrisi et al. 2022), we perform hyperparameter selection on the validation set. NVIDIA A100 GPUs are used for all experiments. Kindly refer to our Appendix for all other details.

**Competitors.** We compare methods from three lines. We first consider the *source-only* ( $\mathcal{S}_{\text{only}}$ ) and *supervised-target* ( $\mathcal{T}_{\text{sup}}$ ) which uses only labeled source data and only labeled target data, respectively. These two baselines serve as the lower and upper bounds for our tasks. Secondly, we consider five popular image-based UDA methods by simply ignoring temporal information, namely DANN (Ganin et al. 2016), JAN (Long et al. 2017), ADDA (Tzeng et al. 2017), AdaBN (Li et al. 2018), and MCD (Saito et al. 2018). Lastly and most importantly, we compare several recent SoTA video-based UDA methods, including TA<sup>3</sup>N (Chen et al. 2019), SAVA (Choi et al. 2020), TCoN (Pan et al. 2020), ABG (Luo et al. 2020), CoMix (Sahoo et al. 2021), CO<sup>2</sup>A (Turrisi et al. 2022), and MA<sup>2</sup>L-TD (Chen, Gao, and Ma 2022). All these methods use the single modality RGB features. We directly quote numbers reported in published papers whenever possible. There exist recent works conducting video-based UDA using multi-modal data, *e.g.*, RGB + Flow. Although *TransVAE* solely uses RGB features, we still take this set of methods into account. Specifically, we consider MM-SADA (Munro and Damen 2020), STCDA (Song et al. 2021), CMCD (Kim et al. 2021), and CIA (Yang et al. 2022).

Table 2: Comparison results on Jester and Epic-Kitchens.

Task	$\mathcal{S}_{\text{only}}$	DANN	ADDA	TA <sup>3</sup> N	CoMix	<b>TransVAE</b>	$\mathcal{T}_{\text{sup}}$
<b>J<sub>S</sub> <math>\rightarrow</math> J<sub>T</sub></b>	51.5	55.4	52.3	55.5	64.7	<b>66.1 (+14.6)</b>	95.6
D <sub>1</sub> $\rightarrow$ D <sub>2</sub>	32.8	37.7	35.4	34.2	42.9	<b>50.5 (+17.7)</b>	64.0
D <sub>1</sub> $\rightarrow$ D <sub>3</sub>	34.1	36.6	34.9	37.4	40.9	<b>50.3 (+16.2)</b>	63.7
D <sub>2</sub> $\rightarrow$ D <sub>1</sub>	35.4	38.3	36.3	40.9	38.6	<b>50.3 (+14.9)</b>	57.0
D <sub>2</sub> $\rightarrow$ D <sub>3</sub>	39.1	41.9	40.8	42.8	45.2	<b>58.6 (+19.5)</b>	63.7
D <sub>3</sub> $\rightarrow$ D <sub>1</sub>	34.6	38.8	36.1	39.9	42.3	<b>48.0 (+13.4)</b>	57.0
D <sub>3</sub> $\rightarrow$ D <sub>2</sub>	35.8	42.1	41.4	44.2	49.2	<b>58.0 (+22.2)</b>	64.0
<b>Average <math>\uparrow</math></b>	35.3	39.2	37.4	39.9	43.2	<b>52.6 (+17.3)</b>	61.5

Table 3: Comparison with methods using multi-modal data.

Task	$\mathcal{S}_{\text{only}}$	MM-SADA	STCDA	CMCD	CIA	<b>TransVAE</b>
U $\rightarrow$ H	86.1	84.2	83.1	84.7	<b>88.3</b>	<b>87.8 (+1.7)</b>
H $\rightarrow$ U	92.5	91.1	92.1	92.8	94.1	<b>99.0 (+6.8)</b>
<b>Average <math>\uparrow</math></b>	89.3	87.7	87.6	88.8	91.2	<b>93.4 (+4.1)</b>
D <sub>1</sub> $\rightarrow$ D <sub>2</sub>	43.2	49.5	52.0	50.3	<b>52.5</b>	<b>50.5 (+7.3)</b>
D <sub>1</sub> $\rightarrow$ D <sub>3</sub>	42.5	44.1	45.5	46.3	47.8	<b>50.3 (+7.8)</b>
D <sub>2</sub> $\rightarrow$ D <sub>1</sub>	43.0	48.2	49.0	49.5	49.8	<b>50.3 (+7.3)</b>
D <sub>2</sub> $\rightarrow$ D <sub>3</sub>	48.0	52.7	52.5	52.0	53.2	<b>58.6 (+10.6)</b>
D <sub>3</sub> $\rightarrow$ D <sub>1</sub>	43.0	50.9	<b>52.6</b>	51.5	52.2	<b>48.0 (+5.0)</b>
D <sub>3</sub> $\rightarrow$ D <sub>2</sub>	55.5	56.1	55.6	56.3	57.6	<b>58.0 (+2.8)</b>
<b>Average <math>\uparrow</math></b>	45.9	50.3	51.2	51.0	52.2	<b>52.6 (+6.7)</b>

### 4.3 Comparative Studies

**Results on UCF-HMDB.** Tab. 1 shows the comparison results of *TransVAE* with baselines and SoTA methods on UCF-HMDB. The best result among all the baselines is highlighted using bold. Overall, methods using I3D backbone achieve better results than those using ResNet-101. Our *TransVAE* consistently outperforms all previous methods. In particular, *TransVAE* achieves 93.37% average accuracy, improving the best competitor CO<sup>2</sup>A (Turrisi et al. 2022), with the same I3D backbone, by 1.38%. Surprisingly, we observe that *TransVAE* even yields better results (by a 2.1% improvement) than the supervised-target ( $\mathcal{T}_{\text{sup}}$ ) baseline. This is because that the H  $\rightarrow$  U task already has a good performance without adaptation, *i.e.*, 88.79% for the source-only ( $\mathcal{S}_{\text{only}}$ ) baseline, and thus the target pseudo-labels used in *TransVAE* are almost correct. By further aligning domains and equivalently augmenting training data, *TransVAE* outperforms  $\mathcal{T}_{\text{sup}}$  which is only trained with target data.

**Results on Jester & Epic-Kitchens.** Tab. 2 shows the comparison results on the Jester and Epic-Kitchens benchmarks. We can see that our *TransVAE* is the clear winner among all the methods on all the tasks. Specifically, *TransVAE* achieves a 1.4% improvement and a 9.4% average improvement over the runner-up baseline CoMix (Sahoo et al. 2021) on Jester and Epic-Kitchens, respectively. This verifies the superiority of *TransVAE* over others in handling video-based UDA. However, we also notice that the accuracy gap between CoMix and  $\mathcal{T}_{\text{sup}}$  is still significant on Jester. This is because the large-scale Jester dataset contains highly heterogeneous data across domains, *e.g.*, the source domain contains videos of the rolling hand forward, while the target domain only consists of videos of the rolling hand backward. This leaves much room for improvement in the future.

**Comparisons with Multi-Modal Methods.** We further

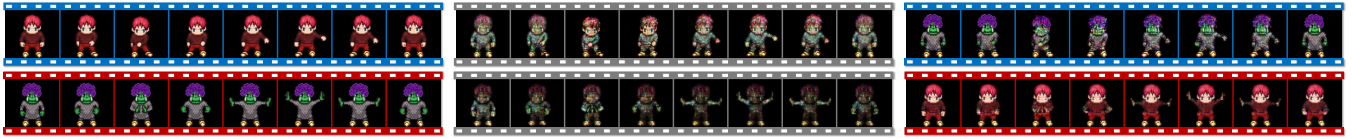


Figure 4: Domain disentanglement and transfer examples. **Left:** Video sequence inputs for  $\mathcal{D} = \mathbf{P}_1$  (“Human”,  $\blacksquare$ ) and  $\mathcal{D} = \mathbf{P}_2$  (“Alien”,  $\blacksquare$ ). **Middle:** Reconstructed sequences ( $\blacksquare$ ) with  $\mathbf{z}_1^{\mathcal{D}}, \dots, \mathbf{z}_T^{\mathcal{D}}$ . **Right:** Domain transferred sequences with exchanged  $\mathbf{z}_d^{\mathcal{D}}$ .

Table 4: Loss separation studies on different video-based UDA tasks by dropping each loss sequentially.

$\mathcal{L}_{\text{svae}}$	$\mathcal{L}_{\text{cls}}$	$\mathcal{L}_{\text{adv}}$	$\mathcal{L}_{\text{mi}}$	$\mathcal{L}_{\text{ctc}}$	PL	$\mathbf{U} \rightarrow \mathbf{H}$	$\mathbf{H} \rightarrow \mathbf{U}$	$\mathbf{J}_S \rightarrow \mathbf{J}_T$	$\mathbf{D}_1 \rightarrow \mathbf{D}_2$	$\mathbf{D}_1 \rightarrow \mathbf{D}_3$	$\mathbf{D}_2 \rightarrow \mathbf{D}_1$	$\mathbf{D}_2 \rightarrow \mathbf{D}_3$	$\mathbf{D}_3 \rightarrow \mathbf{D}_1$	$\mathbf{D}_3 \rightarrow \mathbf{D}_2$	Avg.
✓		✓	✓	✓	✓	18.61	26.62	22.92	34.00	30.29	33.79	30.49	28.51	34.27	28.83
✓	✓		✓	✓	✓	83.06	93.52	48.07	40.93	43.33	43.91	51.13	41.84	52.67	55.38
✓	✓	✓		✓	✓	85.83	93.52	65.12	46.67	48.56	49.43	55.34	45.52	54.53	60.60
✓	✓	✓	✓		✓	83.89	95.80	64.89	48.53	48.25	48.96	54.21	45.52	55.73	60.64
✓	✓	✓	✓	✓		87.22	94.40	64.64	49.87	48.25	49.66	56.47	47.59	55.07	61.46
✓	✓	✓	✓	✓	✓	<b>87.78</b>	<b>98.95</b>	<b>66.10</b>	<b>50.53</b>	<b>50.31</b>	<b>50.34</b>	<b>58.62</b>	<b>48.04</b>	<b>58.00</b>	<b>63.19</b>

compare four very recent video-based UDA methods that use multiple modalities, *i.e.*, RGB features and optical flows, although *TranSVAE* only uses RGB features. Surprisingly, *TranSVAE* is the best in 4 of 6 tasks and achieves better results than the latest SoTA method CIA (Yang et al. 2022). Considering *TranSVAE* only uses single-modal data, we are confident that there exists great potential for further improvements with multi-modal data taken into account.

#### 4.4 Property Analysis

**Disentanglement Analysis.** We analyze the disentanglement effect of *TranSVAE* on Sprites and show results in Fig. 4. The left subfigure shows the original sequences of the two domains. The “Human” and “Alien” are with completely different appearances and the former is *casting spells* while the latter is *slashing*. The middle subfigure shows the sequences reconstructed only using  $\{\mathbf{z}_1^{\mathcal{D}}, \dots, \mathbf{z}_T^{\mathcal{D}}\}$ . It can be clearly seen that the two sequences keep the same action as the corresponding original ones. However, if we only focus on the appearance characteristics, it is difficult to distinguish the domain to which the sequences belong. This indicates that  $\{\mathbf{z}_1^{\mathcal{D}}, \dots, \mathbf{z}_T^{\mathcal{D}}\}$  are indeed *domain-invariant* and well encode the semantic information. The right subfigure shows the sequences reconstructed by exchanging  $\mathbf{z}_d^{\mathcal{D}}$ , which results in two sequences with the same actions but exchanged appearance. This verifies that  $\mathbf{z}_d^{\mathcal{D}}$  is representing the appearance information, which is actually the *domain-related* information in this example. This property study<sup>3</sup> sufficiently supports that *TranSVAE* can successfully disentangle the domain information from other information, with the former embedded in  $\mathbf{z}_d^{\mathcal{D}}$  and the latter embedded in  $\{\mathbf{z}_1^{\mathcal{D}}, \dots, \mathbf{z}_T^{\mathcal{D}}\}$ .

**Ablation Studies.** We now analyze the effectiveness of each loss term in Eq. (14). We compare with four variants of *TranSVAE*, each removing one loss term by equivalently setting the weight  $\lambda$  to 0. The ablation results on UCF-HMDB, Jester, and Epic-Kitchens are shown in Tab. 4. As can be seen, removing  $\mathcal{L}_{\text{cls}}$  significantly reduces the transfer performance in all the tasks. This is reasonable as  $\mathcal{L}_{\text{cls}}$  is used

to discover the discriminative features. Removing any of  $\mathcal{L}_{\text{adv}}$ ,  $\mathcal{L}_{\text{mi}}$ , and  $\mathcal{L}_{\text{ctc}}$  leads to an inferior result than the full *TranSVAE* setup. This demonstrates that every proposed loss matters in our framework. We further conduct another ablation study by sequentially integrating  $\mathcal{L}_{\text{cls}}$ ,  $\mathcal{L}_{\text{adv}}$ ,  $\mathcal{L}_{\text{mi}}$ , and  $\mathcal{L}_{\text{ctc}}$  into our sequential VAE structure. We follow the above integration order based on the average positive improvement that a loss brings to *TranSVAE* as shown in Tab. 4. We further use t-SNE (Van der Maaten and Hinton 2008) to visualize the features learned by these different variants. We plot two sets of t-SNE figures, one using the class-wise label and another using the domain label. Fig. 5 and Fig. 6 show the visualization and the quantitative results. As can be seen from the t-SNE feature visualizations, adding a new component improves both the domain and semantic alignments, and the best alignment is achieved when all the components are considered. The quantitative results further show that the transfer performance gradually increases with the sequential integration of the four components, which again verifies the effectiveness of each component in *TranSVAE*.

## 5 Conclusion

In this paper, we proposed a *TranSVAE* framework for the video-based UDA tasks. Our key idea is to explicitly disentangle the domain information from other information during the adaptation. We developed a novel sequential VAE structure with two sets of latent factors and proposed four constraints to regulate these factors for adaptation purposes. Extensive empirical studies clearly verify that *TranSVAE* consistently offers performance improvements compared with existing state-of-the-art methods. Comprehensive property analysis further demonstrates that *TranSVAE* is an effective and promising method for video-based UDA.

### Public Resources Used

We acknowledge the use of the following public resources, during the course of this work:

- Sprites<sup>4</sup> ..... CC-BY-SA-3.0

<sup>4</sup><https://github.com/YingzhenLi/Sprites>

<sup>3</sup>Try a live demo for domain disentanglement and transfer in *TranSVAE* at: <https://huggingface.co/spaces/ldkong/TranSVAE>.

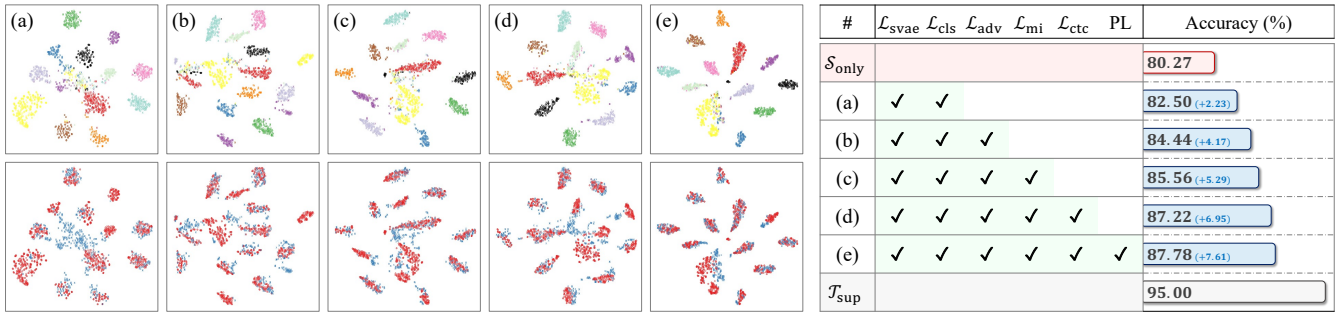


Figure 5: Loss integration studies on  $\mathbf{U} \rightarrow \mathbf{H}$ . **Left:** The t-SNE plots for class-wise (top row) and domain (bottom row, red source & blue target) features. **Right:** Ablation results (%) by adding each loss sequentially, *i.e.*, row (a) - row (e).

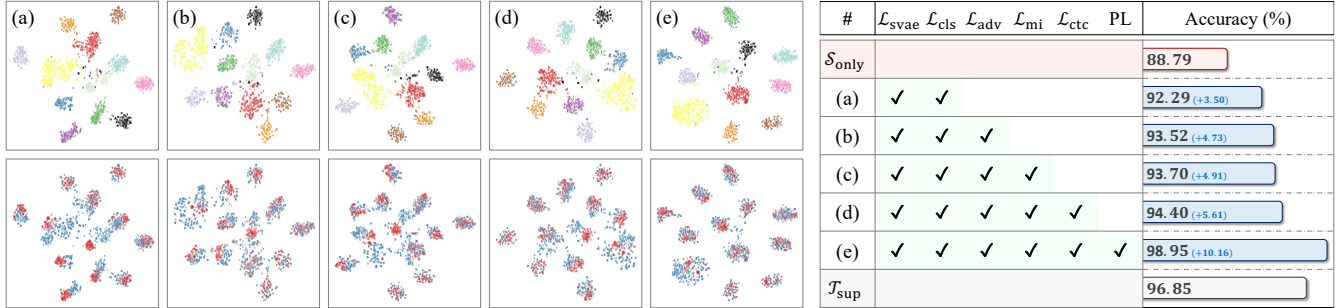


Figure 6: Loss integration studies on  $\mathbf{H} \rightarrow \mathbf{U}$ . **Left:** The t-SNE plots for class-wise (top row) and domain (bottom row, red source & blue target) features. **Right:** Ablation results (%) by adding each loss sequentially, *i.e.*, row (a) - row (e).

- UCF<sub>101</sub><sup>5</sup> ..... Unknown
- HMDB<sub>51</sub><sup>6</sup> ..... CC BY 4.0
- Jester<sup>7</sup> ..... Unknown
- Epic-Kitchens<sup>8</sup> ..... CC BY-NC 4.0
- I3D<sup>9</sup> ..... Apache License 2.0
- TRN<sup>10</sup> ..... BSD 2-Clause License
- Netron<sup>11</sup> ..... MIT License

## References

Bai, J.; Wang, W.; and Gomes, C. P. 2021. Contrastively disentangled sequential variational autoencoder. In *Advances in Neural Information Processing Systems*, volume 34, 10105–10118.

Batina, L.; Gierlichs, B.; Prouff, E.; Rivain, M.; Standaert, F.-X.; and Veyrat-Charvillon, N. 2011. Mutual information analysis: a comprehensive study. *Journal of Cryptology*, 24(2): 269–291.

<sup>5</sup><https://www.crcv.ucf.edu/data/UCF101.php>

<sup>6</sup><https://serre-lab.clps.brown.edu/resource/hmdb-a-large-human-motion-database>

<sup>7</sup><https://20bn.com/datasets/jester>

<sup>8</sup><https://epic-kitchens.github.io/2021>

<sup>9</sup><https://github.com/piergiaj/pytorch-i3d>

<sup>10</sup><https://github.com/zhoubolei/TRN-pytorch>

<sup>11</sup><https://github.com/lutzroeder/netron>

Cai, Q.; Pan, Y.; Ngo, C.-W.; Tian, X.; Duan, L.; and Yao, T. 2019a. Exploring object relation in mean teacher for cross-domain detection. In *IEEE/CVF Conference on Computer Vision and Pattern Recognition*, 11457–11466.

Cai, R.; Li, Z.; Wei, P.; Qiao, J.; Zhang, K.; and Hao, Z. 2019b. Learning disentangled semantic representation for domain adaptation. In *International Joint Conferences on Artificial Intelligence*, volume 2019, 2060.

Cai, R.; Wu, F.; Li, Z.; Wei, P.; Yi, L.; and Zhang, K. 2021. Graph domain adaptation: A generative view. *arXiv preprint arXiv:2106.07482*.

Carreira, J.; and Zisserman, A. 2017. Quo vadis, action recognition? a new model and the kinetics dataset. In *IEEE/CVF Conference on Computer Vision and Pattern Recognition*, 6299–6308.

Chen, M.-H.; Kira, Z.; AlRegib, G.; Yoo, J.; Chen, R.; and Zheng, J. 2019. Temporal attentive alignment for large-scale video domain adaptation. In *IEEE/CVF International Conference on Computer Vision*, 6321–6330.

Chen, P.; Gao, Y.; and Ma, A. J. 2022. Multi-level Attentive Adversarial Learning with Temporal Dilation for Unsupervised Video Domain Adaptation. In *IEEE/CVF Winter Conference on Applications of Computer Vision*, 1259–1268.

Chen, R. T.; Li, X.; Grosse, R. B.; and Duvenaud, D. K. 2018. Isolating sources of disentanglement in variational autoencoders. In *Advances in Neural Information Processing Systems*, volume 31, 1–11.



- Choi, J.; Sharma, G.; Schuler, S.; and Huang, J.-B. 2020. Shuffle and attend: Video domain adaptation. In *European Conference on Computer Vision*, 678–695. Springer.
- Damen, D.; Doughty, H.; Farinella, G. M.; Fidler, S.; Furnari, A.; Kazakos, E.; Moltisanti, D.; Munro, J.; Perrett, T.; Price, W.; et al. 2018. Scaling egocentric vision: The epic-kitchens dataset. In *European Conference on Computer Vision*, 720–736.
- Deng, W.; Zhao, L.; Liao, Q.; Guo, D.; Kuang, G.; Hu, D.; Pietikäinen, M.; and Liu, L. 2021. Informative feature disentanglement for unsupervised domain adaptation. *IEEE Transactions on Multimedia*, 24: 2407–2421.
- Ganin, Y.; Ustinova, E.; Ajakan, H.; Germain, P.; Larochelle, H.; Laviolette, F.; Marchand, M.; and Lempitsky, V. 2016. Domain-adversarial training of neural networks. *Journal of Machine Learning Research*, 17(1): 2096–2030.
- Guan, D.; Huang, J.; Xiao, A.; Lu, S.; and Cao, Y. 2021. Uncertainty-aware unsupervised domain adaptation in object detection. *IEEE Transactions on Multimedia*, 24: 2502–2514.
- Ilse, M.; Tomczak, J. M.; Louizos, C.; and Welling, M. 2020. Diva: Domain invariant variational autoencoders. In *Medical Imaging with Deep Learning*, 322–348. PMLR.
- Kay, W.; Carreira, J.; Simonyan, K.; Zhang, B.; Hillier, C.; Vijayanarasimhan, S.; Viola, F.; Green, T.; Back, T.; Natsev, P.; et al. 2017. The kinetics human action video dataset. *arXiv preprint arXiv:1705.06950*.
- Kim, D.; Tsai, Y.-H.; Zhuang, B.; Yu, X.; Sclaroff, S.; Saenko, K.; and Chandraker, M. 2021. Learning cross-modal contrastive features for video domain adaptation. In *IEEE/CVF International Conference on Computer Vision*, 13618–13627.
- Kong, L.; Quader, N.; Liong, V. E.; and Zhang, H. 2021. ConDA: Unsupervised domain adaptation for LiDAR segmentation via regularized domain concatenation. *arXiv preprint arXiv:2111.15242*.
- Kuehne, H.; Jhuang, H.; Garrote, E.; Poggio, T.; and Serre, T. 2011. HMDB: a large video database for human motion recognition. In *IEEE/CVF International Conference on Computer Vision*, 2556–2563. IEEE.
- Li, Y.; and Mandt, S. 2018. Disentangled sequential autoencoder. In *International Conference on Machine Learning*, 5670–5679. PMLR.
- Li, Y.; Wang, N.; Shi, J.; Hou, X.; and Liu, J. 2018. Adaptive batch normalization for practical domain adaptation. *Pattern Recognition*, 80: 109–117.
- Long, M.; Zhu, H.; Wang, J.; and Jordan, M. I. 2017. Deep transfer learning with joint adaptation networks. In *International Conference on Machine Learning*, 2208–2217. PMLR.
- Luo, Y.; Huang, Z.; Wang, Z.; Zhang, Z.; and Baktashmotlagh, M. 2020. Adversarial bipartite graph learning for video domain adaptation. In *ACM International Conference on Multimedia*, 19–27.
- Materzynska, J.; Berger, G.; Bax, I.; and Memisevic, R. 2019. The jester dataset: A large-scale video dataset of human gestures. In *IEEE/CVF International Conference on Computer Vision Workshops*, 1–12.
- Munro, J.; and Damen, D. 2020. Multi-modal domain adaptation for fine-grained action recognition. In *IEEE/CVF Conference on Computer Vision and Pattern Recognition*, 122–132.
- Pan, B.; Cao, Z.; Adeli, E.; and Niebles, J. C. 2020. Adversarial cross-domain action recognition with co-attention. In *AAAI Conference on Artificial Intelligence*, 11815–11822.
- Sahoo, A.; Shah, R.; Panda, R.; Saenko, K.; and Das, A. 2021. Contrast and mix: Temporal contrastive video domain adaptation with background mixing. In *Advances in Neural Information Processing Systems*, volume 34, 23386–23400.
- Saito, K.; Watanabe, K.; Ushiku, Y.; and Harada, T. 2018. Maximum classifier discrepancy for unsupervised domain adaptation. In *IEEE/CVF Conference on Computer Vision and Pattern Recognition*, 3723–3732.
- Saporta, A.; Douillard, A.; Vu, T.-H.; Pérez, P.; and Cord, M. 2022. Multi-Head Distillation for Continual Unsupervised Domain Adaptation in Semantic Segmentation. In *IEEE/CVF Conference on Computer Vision and Pattern Recognition*, 3751–3760.
- Song, X.; Zhao, S.; Yang, J.; Yue, H.; Xu, P.; Hu, R.; and Chai, H. 2021. Spatio-temporal contrastive domain adaptation for action recognition. In *IEEE/CVF Conference on Computer Vision and Pattern Recognition*, 9787–9795.
- Soomro, K.; Zamir, A. R.; and Shah, M. 2012. UCF101: A dataset of 101 human actions classes from videos in the wild. *arXiv preprint arXiv:1212.0402*.
- Turrisi, V. G.; Zara, G.; Rota, P.; Oliveira-Santos, T.; Sebe, N.; Murino, V.; and Ricci, E. 2022. Dual-Head Contrastive Domain Adaptation for Video Action Recognition. In *IEEE/CVF Winter Conference on Applications of Computer Vision*, 2234–2243.
- Tzeng, E.; Hoffman, J.; Saenko, K.; and Darrell, T. 2017. Adversarial discriminative domain adaptation. In *IEEE/CVF Conference on Computer Vision and Pattern Recognition*, 7167–7176.
- Van der Maaten, L.; and Hinton, G. 2008. Visualizing data using t-SNE. *Journal of Machine Learning Research*, 9(11).
- Wang, X.; and Gupta, A. 2018. Videos as space-time region graphs. In *European Conference on Computer Vision*, 399–417.
- Wilson, G.; and Cook, D. J. 2020. A survey of unsupervised deep domain adaptation. *ACM Transactions on Intelligent Systems and Technology*, 11(5): 1–46.
- Xiao, N.; and Zhang, L. 2021. Dynamic weighted learning for unsupervised domain adaptation. In *IEEE/CVF Conference on Computer Vision and Pattern Recognition*, 15242–15251.
- Yang, L.; Huang, Y.; Sugano, Y.; and Sato, Y. 2022. Interact Before Align: Leveraging Cross-Modal Knowledge for Domain Adaptive Action Recognition. In *IEEE/CVF Conference on Computer Vision and Pattern Recognition*, 14722–14732.

- Yu, F.; Wang, D.; Chen, Y.; Karianakis, N.; Shen, T.; Yu, P.; Lymberopoulos, D.; Lu, S.; Shi, W.; and Chen, X. 2022. SC-UDA: Style and Content Gaps aware Unsupervised Domain Adaptation for Object Detection. In *IEEE/CVF Winter Conference on Applications of Computer Vision*, 382–391.
- Yu, Y.; Gong, Z.; Zhong, P.; and Shan, J. 2017. Unsupervised representation learning with deep convolutional neural network for remote sensing images. In *International Conference on Image and Graphics*, 97–108. Springer.
- Zhang, J.; Huang, J.; Tian, Z.; and Lu, S. 2022. Spectral unsupervised domain adaptation for visual recognition. In *IEEE/CVF Conference on Computer Vision and Pattern Recognition*, 9829–9840.
- Zhou, B.; Andonian, A.; Oliva, A.; and Torralba, A. 2018. Temporal relational reasoning in videos. In *European Conference on Computer Vision*, 803–818.
- Zhu, Y.; Min, M. R.; Kadav, A.; and Graf, H. P. 2020. S3vae: Self-supervised sequential vae for representation disentanglement and data generation. In *IEEE/CVF Conference on Computer Vision and Pattern Recognition*, 6538–6547.
- Zou, Y.; Yu, Z.; Kumar, B.; and Wang, J. 2018. Unsupervised domain adaptation for semantic segmentation via class-balanced self-training. In *European Conference on Computer Vision*, 289–305.